Hindawi
International Journal of Aerospace Engineering
Volume 2019, Article ID 8056342, 17 pages
https://doi.org/10.1155/2019/8056342

Research Article

Profile-Tracking-Based Adaptive Guidance Law against Maneuvering Targets

Jingshuai Huang[1], **Hongbo Zhang**[1], **Guojian Tang**[1] and **Weimin Bao**[1,2]

[1]*College of Aerospace Science and Engineering, National University of Defense Technology, Changsha 410073, China*
[2]*China Aerospace Science and Technology Corporation, Beijing 100048, China*

Correspondence should be addressed to Hongbo Zhang; zhanghb1304@nudt.edu.cn

Received 26 March 2019; Revised 8 September 2019; Accepted 3 October 2019; Published 30 November 2019

Academic Editor: Seid H. Pourtakdoust

For the terminal guidance problem of a missile intercepting a maneuvering target, a profile-tracking-based adaptive guidance law is proposed with inherent continuity in this paper. To flexibly and quantitatively control the convergence rate of the line-of-sight rate, a standard tracking profile is designed where the convergence rate is analytically given. Then, a nonsingular fast terminal sliding-mode control approach is used to track the profile. By estimating the square of the upper bound of target maneuver, an adaptive term is constructed to compensate the maneuver. Therefore, no information of target acceleration is required in the derived law. Stability analysis shows that the tracking error can converge to a small neighborhood of zero in finite time. Furthermore, a guidance-command-conversion scheme is presented to convert the law into the one appropriate for endoatmospheric interceptions. Simulation results indicate that the proposed law is effective and outperforms existing guidance laws.

1. Introduction

The terminal guidance law of a missile plays a crucial role in making a successful intercept, and the guidance performance of the law exerts a direct influence on miss distance, control efforts, etc. Proportional navigation (PN) and its variants are widely applied in a considerable variety of intercept engagements due to inherent simplicity and high effectiveness [1–3]. However, with enhancement of target maneuverability, PN suffers from a significant degradation of intercept performance because of limited capability to suppress rotation of the line of sight (LOS) between a missile and a target induced by target maneuver. Then, the augmented PN was proposed to compensate target maneuver, but the price paid is the information of target acceleration which cannot be measured directly and is difficult to be accurately estimated [4, 5]. To meet the challenge of precisely intercepting agile targets, some advanced control algorithms have been used to develop robust guidance laws, such as sliding mode control [6–11], nonlinear H_∞ control [12], dynamic surface control [13], and finite time control [14–18].

Sliding mode control (SMC) is a simple and effective approach to handling external disturbances and system uncertainties, which attracts considerable attention paid to applying SMC to intercept guidance. The SMC-based guidance law can achieve the robustness to target maneuver and consequently outperforms the PN law [6–11]. However, most of the SMC-based guidance laws provide only the asymptotic or exponential stability of a guidance system, which indicates that the LOS rate (LOSR) is driven to zero or its small neighborhood only as time approaches infinity. Since the terminal phase of interception is of short duration, it is the convergence property of the LOSR that is a main influence on guidance performance. Compared with the asymptotic stability, the finite-time stability firstly proposed in 1986 demonstrates that a dynamical system from an unstable state can converge to its equilibrium point in finite time [19–21]. In recent years, driving the LOSR to zero or its small neighborhood in finite time has become increasingly prevalent during the design of a guidance law. On basis of the finite-time stability theory [20], the finite-time guidance law was designed in [14–16] which obtained high accuracy and

good performance. To acquire the robustness to target maneuver, the aforementioned guidance laws require the introduction of a discontinuous switching term whose gain is generally larger than the upper bound of target maneuver. However, the term is followed by chattering of guidance command, and the bound is difficult to be accurately given in most cases. To alleviate chattering, a common technique is to employ a continuous function instead of the signum function in the switching term, such as the sigmoid function [8] and the saturation function [14].

In the design of the guidance law against maneuvering targets, the approach is crucial to addressing target maneuver which is generally considered as a bounded external disturbance with respect to a guidance system. It is known that the way to introduce a switching term easily brings about chattering. Then, estimation and adaptive control theories are adopted to deal with target maneuver in [22–29]. A nonhomogeneous disturbance observer was used to estimate disturbances in a guidance system, and the chattering was eliminated in [22]. Ma and Zhang [23] proposed a finite-time convergent guidance law, and the target maneuver was estimated using an extended state observer and compensated. However, the finite-time stability theory was no longer strictly satisfied due to the presence of an estimation error. Based on the finite-time stability theory and a nonlinear disturbance observer, Zhang et al. [24] presented a composite guidance law where the gain of the switching term was reduced to being only larger than the upper bound of a disturbance estimation error. The finite-time convergent characteristic of the LOSR was proven under the composite law. In [25], a finite-time guidance law was given without the bound knowledge of a disturbance estimation error by an adaptive exponential reaching law. Different from the observer method in [22–27] considered the target maneuver as a disturbance with unknown bound and employed an adaptive algorithm to approach the bound. Furthermore, the proposed controllers for a guidance system were inherently continuous by substituting the saturation function for the sign function and asymptotically converged to the origin in theory in spite of the substitution. In [28], an adaptive nonlinear guidance law was developed, and two adaptive terms were involved to estimate target acceleration. Although the finite-time convergence of the LOSR was guaranteed to zero, the convergence process was of long duration and the bounds of target acceleration and jerk were required. By combining nonsingular terminal SMC and adaptive control, Zhou and Yang [29] constructed an adaptive finite-time guidance law which contained an adaptive continuous term to reject target maneuver. Without the information of target acceleration, it was ensured that the system state could converge to a small neighborhood of zero. In terms of robust guidance laws, the antichattering and the finite-time convergence of the LOSR are two significant qualities. From the previous discussions, the chattering problem has been solved well and the finite-time convergence can be guaranteed in theory and simulation senses. However, the convergence time is difficult to be quantitatively controlled. Moreover, the simple but radical concept is embraced that the LOSR decreases as rapidly as possible. Sometimes, a rapid convergence may be unnecessary which signifies more control efforts in most cases.

Based on the above discussions, this paper is devoted to flexibly and accurately regulate the convergence rate of the LOSR in considering of saving energy consumption. Then, a novel profile-tracking-based adaptive guidance law is proposed against maneuvering targets with inherent continuity. The main contributions of this paper are summarized as follows: (1) a standard tracking profile is designed which describes the convergence rate of the LOSR analytically. A nonsingular fast terminal SMC method is employed to track the profile. (2) An inherently continuous adaptive term is constructed to compensate target maneuver without the information of target acceleration. The finite-time convergence to a small neighborhood of zero is strictly guaranteed of the tracking error. (3) To be suitable for endoatmospheric interceptions, a guidance-command-conversion scheme is put forward to change the action orientation of guidance command. Compared with existing guidance laws, the proposed law has smaller miss distance and less control efforts.

The rest of this paper is organized as follows. The following section gives the modeling description of intercept guidance. Section 3 presents a standard tracking profile. In Section 4, a novel profile-tracking-based adaptive guidance law is derived in details. Numerical simulations are performed in Section 5, followed by conclusions in Section 6.

2. Preliminaries

An appropriate coordinate system is conducive to revealing relative-motion characteristics between a missile and a target and simplifying the design of a guidance law. In existing literatures, there are mainly two coordinate systems used to describe intercept engagement. One is the commonly used spherical LOS coordinate system, as shown in [9]. The other is the rotating LOS coordinate system proposed in [5]. In this paper, we adopt the rotating LOS coordinate system where a decoupled relative-motion equation set is obtained.

The three-dimensional engagement geometry is presented in Figure 1 where a missile M is intercepting a maneuvering target T. The missile and the target are assumed as point masses. $o_I x_I y_I z_I$ represents the inertial reference frame. $\mathbf{v}_m$ and $\mathbf{v}_t$ denote the velocities of the missile and the target, respectively.

From Figure 1, we have

$$\mathbf{r} = \mathbf{r}_t - \mathbf{r}_m = r\mathbf{e}_r, \tag{1}$$

where r is the missile-target relative distance and $\mathbf{e}_r$ is the unit vector along the LOS. Orientation variation of the target relative to the missile brings about rotation of the LOS. However, the LOS rotation is completely dependent on the components of $\mathbf{v}_m$ and $\mathbf{v}_t$ normal to the LOS. Therefore, angular velocity of the LOS rotation is perpendicular to the LOS and denoted as $\boldsymbol{\omega}$. Then, $\boldsymbol{\omega}$ is computed as

$$\boldsymbol{\omega} = \frac{\mathbf{r} \times \mathbf{v}}{r^2} = \omega \mathbf{e}_\omega, \quad \omega \geq 0, \tag{2}$$

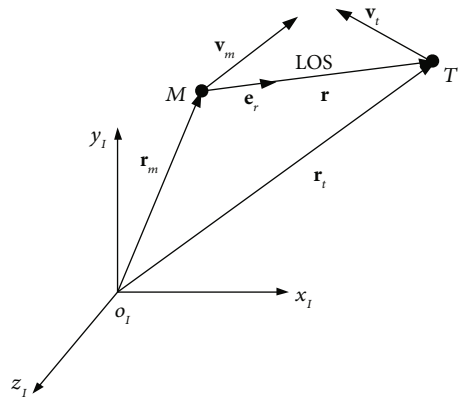

Figure 1: Three-dimensional engagement geometry.

where $\mathbf{v} = \mathbf{v}_t - \mathbf{v}_m$, $\mathbf{e}_\omega$ is the unit vector along $\boldsymbol{\omega}$, and ω, the length of $\boldsymbol{\omega}$, is known as the LOSR. Taking the derivative of (1) yields

$$\mathbf{v} = v_r \mathbf{e}_r + v_\theta (\mathbf{e}_\omega \times \mathbf{e}_r), \tag{3}$$

where $v_r = \dot{r}$ is the closing velocity and $v_\theta = r\omega$ is the component of $\mathbf{v}$ normal to the LOS.

Let $\mathbf{e}_\theta = \mathbf{e}_\omega \times \mathbf{e}_r$, and then the set $(\mathbf{e}_r, \mathbf{e}_\theta, \mathbf{e}_\omega)$ is the unit vectors along the axes of the rotating LOS coordinate system. According to [5], we have the following relations:

$$\begin{cases} \dfrac{d\mathbf{e}_r}{dt} = \omega \mathbf{e}_\theta, \\ \dfrac{d\mathbf{e}_\theta}{dt} = -\omega \mathbf{e}_r + \Omega \mathbf{e}_\theta, \\ \dfrac{d\mathbf{e}_\omega}{dt} = -\Omega \mathbf{e}_\theta, \end{cases} \tag{4}$$

where Ω is the projection along $\mathbf{e}_\theta$ of the rotational angular velocity of $\mathbf{e}_\omega$. Then, the relative-motion equation set in the rotating LOS frame is obtained as

$$\begin{cases} \ddot{r} - r\omega^2 = a_{tr} - a_{mr}, \\ r\dot{\omega} + 2\dot{r}\omega = a_{t\theta} - a_{m\theta}, \\ r\omega\Omega = a_{t\omega} - a_{m\omega}, \end{cases} \tag{5}$$

where $(a_{tr}, a_{t\theta}, a_{t\omega})$ and $(a_{mr}, a_{m\theta}, a_{m\omega})$ are the acceleration components of the target and the missile, respectively. As shown in (5), the first two equations are decoupled from the third equation. For more details, refer to [5].

Before proceeding with the guidance law design, the following assumptions are made.

Assumption 1. Consider that the target acceleration cannot be infinite in practice. Then, it is reasonable to suppose that its magnitude $a_t = \sqrt{a_{tr}^2 + a_{t\theta}^2 + a_{t\omega}^2}$ is bounded, i.e., $a_t \le d$, where d is difficult to be precisely determined prior in practical interceptions. Thus, in the subsequent design, it is regarded as an unknown parameter to be estimated.

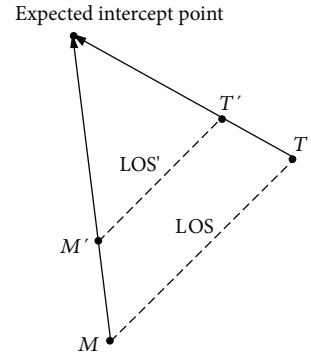

Figure 2: Collision triangle between the missile and the target.

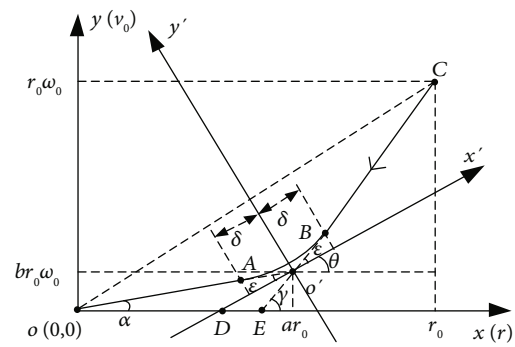

Figure 3: Standard tracking profile of v_θ versus r.

Assumption 2. After the handover from the midcourse to the terminal guidance, the closing velocity $\dot{r}$ satisfies $\dot{r}(t_0) \le -L < 0$, where t_0 is the initial time of terminal guidance and L is a positive constant.

3. Standard Tracking Profile

The typical design principle of a guidance law is that nullifying the LOSR results in the missile being in a desired collision triangle with the target, as described in Figure 2 where the LOSR is zero [7]. The lines of sight are parallel to each other at different instants. It is indicated that the relative motion between the missile and the target is in line with the LOS and a direct collision occurs in the end.

According to the principle, the guidance problem is to find an efficient commanded acceleration $a_{m\theta}$ in (5), which reduces ω to zero. In practical interceptions, however, it is almost impossible that the collision triangle is strictly satisfied because of the initial nonzero LOSR and random target maneuver. In fact, reducing the LOSR to a low level is adequate for performing a collision because of the body sizes of the missile and the target. Motivated by the concept of the standard profile tracking in the trajectory generation of entry vehicles [30], we introduce a standard profile of v_θ versus r into the guidance law design, as shown in Figure 3.

In Figure 3, the profile is composed of $\overline{CB}$, $\overset{\frown}{BA}$, and $\overline{Ao}$. A and B are points of tangency. Since $\overline{CB}$ and $\overline{Ao}$ are line segments, the analytical expressions are written as

$$\begin{cases} \overline{CB} : y = \tan\gamma(x - ar_0) + br_0\omega_0, \quad \gamma = \arctan\dfrac{\omega_0(1-b)}{1-a}, \\ \overline{Ao} : y = \tan\alpha \cdot x, \quad \alpha = \arctan\dfrac{b\omega_0}{a}, \\ \quad a \geq b, \end{cases} \tag{6}$$

where r_0 and ω_0 are the values of r and ω at t_0, respectively. If $a = b$, ω is a constant; if $a > b$, ω decreases in $\overline{CB}$ and keeps constant in $\overline{Ao}$; if $a < b$, ω increases in $\overline{CB}$ and keeps constant in $\overline{Ao}$. Therefore, $a > b$ should be met and b is sufficiently small, which reduces ω to a low level and keeps it constant. In $x'o'y'$, $\widehat{BA}$ is a parabola segment, and the function expression is defined by

$$y' = ex'^2 + f, \quad x' \in [-\delta, \delta]. \tag{7}$$

From Figure 3, the coefficients satisfy the following equations:

$$\begin{cases} 2e\delta = \tan\varepsilon = k, \\ e\delta^2 + f = k\delta, \end{cases} \tag{8}$$

where $\varepsilon = (\gamma - \alpha)/2$. Hence, $e = k/2\delta$, and $f = k\delta/2$. To obtain the function expression of $\widehat{BA}$ in xoy, according to Figure 3, we can give the coordinate transformation from xoy to $x'o'y'$ in the form of

$$\begin{bmatrix} x' \\ y' \end{bmatrix} = \begin{bmatrix} X\cos\theta + Y\sin\theta \\ -X\sin\theta + Y\cos\theta \end{bmatrix}, \tag{9}$$

where $\theta = (\gamma + \alpha)/2$, $X = x - ar_0$, and $Y = y - br_0\omega_0$. Then, substituting (9) into (7), we have

$$\begin{aligned} &k\sin^2\theta Y^2 + 2(kX\cos\theta\sin\theta - \delta\cos\theta)Y \\ &\quad + kX^2\cos^2\theta + 2\delta X\sin\theta + k\delta^2 = 0. \end{aligned} \tag{10}$$

The solution to Y is given by

$$Y = \frac{(\delta\cos\theta - kX\cos\theta\sin\theta) \pm \sqrt{\delta^2\cos^2\theta(1 - k^2\tan^2\theta) - 2kX\delta\sin\theta}}{k\sin^2\theta}. \tag{11}$$

Based on the derivative rule of the implicit function, taking the derivative of (10) with respect to x yields

$$\frac{dy}{dx} = \frac{Z\cos\theta + \sin\theta}{\cos\theta - Z\sin\theta}, \quad Z = \frac{k}{\delta}[(x - ar_0)\cos\theta + (y - br_0\omega_0)\sin\theta]. \tag{12}$$

By examining the left and right derivatives of A and B, it is known that the designed profile is continuously differentiable. The change trend of the profile is formulated as the parameters a, b, and δ. Generally, δ is set as a small constant. When an accurate profile tracking is guaranteed, we can flexibly control the convergence rate of the LOSR by adjusting a and b.

4. Adaptive Guidance Law Based on Profile Tracking

4.1. Guidance Law Design. To accurately track the profile, we define the tracking error as

$$v_e = v_\theta - v_{\theta c}, \tag{13}$$

where $v_{\theta c}$, the standard value of v_θ, is given by the profile. Taking the derivative of (13) and applying the second equation of (5) to the resulting equation, we have

$$\dot{v}_e = -\dot{r}\omega - \dot{r}\frac{dv_{\theta c}}{dr} + a_{t\theta} - a_{m\theta}. \tag{14}$$

Then, (13) and (14) describe a second-order nonlinear system as follows:

$$\begin{cases} \dot{x}_1 = x_2, \\ \dot{x}_2 = -\dot{r}\omega - \dot{r}\dfrac{dv_{\theta c}}{dr} + a_{t\theta} - a_{m\theta}, \end{cases} \tag{15}$$

where the state vector $\mathbf{x}$ is selected as $\mathbf{x} = [x_1, x_2]^{\mathrm{T}} = [\int_0^t v_e(\tau)d\tau, v_e]^{\mathrm{T}}$, $a_{m\theta}$ is the control input, and $a_{t\theta}$ is considered as the system disturbance.

Introduce a nonsingular fast terminal sliding-mode surface defined in [31] as follows:

$$s = x_2 + \alpha_1 x_1 + \alpha_2\beta(x_1), \tag{16}$$

where $\alpha_1, \alpha_2 > 0$, and $\beta(x_1)$ takes the form of

$$\beta(x_1) = \begin{cases} |x_1|^\gamma \operatorname{sgn}(x_1), & |x_1| > \xi, \\ b_1 x_1 + b_2 \operatorname{sgn}(x_1)x_1^2, & |x_1| \leq \xi, \end{cases} \tag{17}$$

where $0 < \gamma < 1$, $b_1 = (2 - \gamma)\xi^{\gamma-1}$, $b_2 = (\gamma - 1)\xi^{\gamma-2}$, $\operatorname{sgn}(\cdot)$ denotes the sign function, and ξ is a small positive constant. The derivative of (17) with respect to x_1 is

$$\frac{d\beta(x_1)}{dx_1} = \begin{cases} \gamma|x_1|^{\gamma-1}, & |x_1| > \xi, \\ b_1 + 2b_2|x_1|, & |x_1| \leq \xi, \end{cases} \tag{18}$$

From (18), it is known that $d\beta(x_1)/dx_1$ is continuous. By using (15), the time derivative of the sliding-mode surface (16) is written as

$$\dot{s} = -\dot{r}\omega - \dot{r}\frac{dv_{\theta c}}{dr} + a_{t\theta} - a_{m\theta} + \alpha_1 x_2 + \alpha_2 x_2 \frac{d\beta(x_1)}{dx_1}. \tag{19}$$

To make the system states converge to the designed sliding-mode surface $s = 0$ in finite time, the following fast reaching law is adopted:

$$\dot{s} = -k_1 s - k_2 |s|^{\mu} \operatorname{sgn}(s), \tag{20}$$

where $k_1, k_2 > 0$, and $0 < \mu < 1$. Substituting (20) into (19), we achieve a guidance law as follows:

$$\begin{aligned} a_{m\theta} = &-\dot{r}\omega - \dot{r}\frac{dv_{\theta c}}{dr} + \alpha_1 x_2 + \alpha_2 x_2 \frac{d\beta(x_1)}{dx_1} \\ &+ k_1 s + k_2 |s|^{\mu} \operatorname{sgn}(s) + a_{t\theta}. \end{aligned} \tag{21}$$

In practical intercepts, the target acceleration $a_{t\theta}$ is difficult to be obtained. From Assumption 1, we have $|a_{t\theta}| \le d_\theta$ where d_θ is unknown. To acquire the robustness to $a_{t\theta}$ and avoid the introduction of switching term, an adaptive term is constructed with inherent continuity [29]. The adaptive guidance law is designed as

$$\begin{aligned} a_{m\theta} = &-\dot{r}\omega - \dot{r}\frac{dv_{\theta c}}{dr} + \alpha_1 x_2 + \alpha_2 x_2 \frac{d\beta(x_1)}{dx_1} \\ &+ k_1 s + k_2 |s|^{\mu} \operatorname{sgn}(s) + \frac{\widehat{\kappa} s}{2\varepsilon^2}, \end{aligned} \tag{22}$$

where $\varepsilon > 0$, $\widehat{\kappa}$ is the estimation of κ, and $\kappa = d_\theta^2$. The updating law of $\widehat{\kappa}$ is given by

$$\dot{\widehat{\kappa}} = k_3 \left(\frac{s^2}{2\varepsilon^2} - k_4 \widehat{\kappa} \right), \tag{23}$$

where $k_3,\ k_4 > 0$.

4.2. Stability Analysis. In this subsection, the stability analysis of the adaptive guidance law is performed. First, we give the following lemma required in the analysis.

Lemma 1 [21]. *Suppose that there is a continuously differentiable and positive definite function $V(\mathbf{x})$ defined in a neighborhood $\mathbf{U} \subset \mathbf{R}^n$ of the origin and that $\dot{V}(\mathbf{x}) \le -pV(\mathbf{x}) - qV^{\eta}(\mathbf{x})$ where $p, q > 0$, and $0 < \eta < 1$, then, $\mathbf{x}$ converges to zero in finite time and the settling time T satisfies the inequality*

$$T \le \frac{1}{p(1-\eta)} \ln \frac{pV^{1-\eta}(\mathbf{x}_0) + q}{q}, \tag{24}$$

where $\mathbf{x}(t_0) = \mathbf{x}_0$.

Theorem 1. *For the guidance system (15) with the sliding-mode surface (16), if the guidance law is chosen as (22) with the updating law (23), then the sliding-mode variable s and the system states x_1 and x_2 will converge to the regions*

$$\begin{aligned} |s| &\le \left(\frac{\varepsilon^2}{2k_2} \right)^{1/(\mu+1)} = \Theta_1, \\ |x_1| &\le \max\left\{ \left(\frac{\Theta_1}{\alpha_2} \right)^{1/\gamma}, \xi \right\} = \Theta_2, \\ |x_2| &\le \Theta_1 + \alpha_1 \Theta_2 + \alpha_2 \Theta_2^{\gamma} \end{aligned} \tag{25}$$

in finite time, respectively.

Proof. Consider the Lyapunov function

$$V_1 = \frac{1}{2} s^2 + \frac{1}{2k_3} \tilde{\kappa}^2, \tag{26}$$

where $\tilde{\kappa} = \kappa - \widehat{\kappa}$. Its time derivative is

$$\dot{V}_1 = s\dot{s} - \frac{1}{k_3} \tilde{\kappa} \dot{\widehat{\kappa}}. \tag{27}$$

Substituting (22) into (19) yields

$$\dot{s} = a_{t\theta} - k_1 s - k_2 |s|^{\mu} \operatorname{sgn}(s) - \frac{\widehat{\kappa} s}{2\varepsilon^2}. \tag{28}$$

By using (23) and (28), (27) is written as

$$\begin{aligned} \dot{V}_1 &= a_{t\theta} s - k_1 s^2 - k_2 |s|^{\mu+1} - \frac{\widehat{\kappa} s^2}{2\varepsilon^2} - \frac{\tilde{\kappa} s^2}{2\varepsilon^2} + k_4 (\kappa - \tilde{\kappa}) \tilde{\kappa} \\ &\le d_\theta |s| - \frac{\kappa s^2}{2\varepsilon^2} - k_1 s^2 - k_2 |s|^{\mu+1} + k_4 |\kappa \tilde{\kappa}| - k_4 \tilde{\kappa}^2. \end{aligned} \tag{29}$$

Noting that

$$\begin{aligned} d_\theta |s| &= 2\sqrt{\frac{\kappa s^2}{2\varepsilon^2} \cdot \frac{\varepsilon^2}{2}} \le \frac{\kappa s^2}{2\varepsilon^2} + \frac{\varepsilon^2}{2}, \\ |\tilde{\kappa}\kappa| &= 2\sqrt{\frac{\rho \tilde{\kappa}^2}{2} \cdot \frac{\kappa^2}{2\rho}} \le \frac{\rho \tilde{\kappa}^2}{2} + \frac{\kappa^2}{2\rho}, \end{aligned} \tag{30}$$

where $0 < \rho < 2$, we can obtain

$$\begin{aligned} \dot{V}_1 &\le -k_1 s^2 - k_2 |s|^{\mu+1} - k_4 \left(1 - \frac{\rho}{2} \right) \tilde{\kappa}^2 + \frac{\varepsilon^2}{2} + k_4 \frac{\kappa^2}{2\rho} \\ &\le -2k_1 \frac{1}{2} s^2 - 2k_3 k_4 \left(1 - \frac{\rho}{2} \right) \frac{1}{2k_3} \tilde{\kappa}^2 + \frac{\varepsilon^2}{2} + k_4 \frac{\kappa^2}{2\rho} \\ &\le -\chi V_1 + \psi, \end{aligned} \tag{31}$$

where $\chi = \min\{2k_1, 2k_3 k_4 (1 - \rho/2)\}$ and $\psi = (k_4 \kappa^2/\rho + \varepsilon^2)/2$. From (31), we have $\dot{V}_1 < 0$ when $V_1 > \psi/\chi$. Thus, V_1 is bounded, and then $\tilde{\kappa}$ is bounded, that is, $|\tilde{\kappa}| \le \zeta$ where ζ is a nonnegative constant. Reconsidering the Lyapunov function $V_2 = s^2/2$, and differentiating V_2 with respect to time, we have

$$\begin{aligned}\dot{V}_2 &\le d_\theta|s| - \frac{\widehat{\kappa}s^2}{2\varepsilon^2} - k_1 s^2 - k_2|s|^{\mu+1} \\ &\le \frac{\tilde{\kappa}s^2}{2\varepsilon^2} + \frac{\varepsilon^2}{2} - k_1 s^2 - k_2|s|^{\mu+1} \\ &\le \frac{\zeta s^2}{2\varepsilon^2} + \frac{\varepsilon^2}{2} - k_1 s^2 - k_2|s|^{\mu+1} \\ &= -2\left(k_1 - \frac{\zeta}{2\varepsilon^2}\right) V_2 - 2^{(\mu+1)/2}\left(k_2 - \frac{\varepsilon^2}{2|s|^{\mu+1}}\right) {V_2}^{(\mu+1)/2}.\end{aligned} \tag{32}$$

According to (32), when $k_1 > \zeta/2\varepsilon^2$ and $k_2 > \varepsilon^2/2|s|^{\mu+1}$, V_2 satisfies Lemma 1. Therefore, s will, in finite time, converge to the region

$$|s| \le \left(\frac{\varepsilon^2}{2k_2}\right)^{1/(\mu+1)} = \Theta_1. \tag{33}$$

After that, the system states satisfy the following equation:

$$x_2 + \alpha_1 x_1 + \alpha_2 \beta(x_1) = s, \quad |s| \le \Theta_1. \tag{34}$$

When $|x_1| \ge \xi$, (34) can be rewritten as

$$x_2 + \alpha_1 x_1 + \left[\alpha_2 - \frac{s}{|x_1|^\gamma \operatorname{sgn}(x_1)}\right] |x_1|^\gamma \operatorname{sgn}(x_1) = 0. \tag{35}$$

Choose the Lyapunov function

$$V_3 = \frac{1}{2} x_1^2. \tag{36}$$

Then, taking the derivative of (36) with respect to time and substituting (35) into the resulting equation, we obtain

$$\dot{V}_3 = -2\alpha_1 V_3 - 2^{(\gamma+1)/2}\left[\alpha_2 - \frac{s}{|x_1|^\gamma \operatorname{sgn}(x_1)}\right] {V_3}^{(\gamma+1)/2}. \tag{37}$$

From Lemma 1, x_1 will converge towards zero when

$$\alpha_2 \ge \frac{\Theta_1}{|x_1|^\gamma}. \tag{38}$$

Thus, the convergence region of x_1 is obtained as

$$|x_1| \le \max\left\{\left(\frac{\Theta_1}{\alpha_2}\right)^{1/\gamma}, \xi\right\} = \Theta_2. \tag{39}$$

Simultaneously, the convergence region of x_2 is given as

$$|x_2| \le |s| + \alpha_1|x_1| + \alpha_2|\beta(x_1)| \le \Theta_1 + \alpha_1\Theta_2 + \alpha_2{\Theta_2}^\gamma. \tag{40}$$

The proof is complete.

4.3. Guidance Command Conversion. According to the implementation direction of guidance acceleration, the existing intercept laws may be mainly classified into two categories. The one category consists of interceptor velocity referenced laws, and the second is referenced to the LOS [32]. On account of the difference in overload-generated pattern, the velocity-referenced guidance system is employed inside the atmosphere by aerodynamically controlled interceptors or interceptors with compound control, while the LOS-referenced one is adopted by the exoatmospheric interceptor which generates overload by body-installed lateral jet engines [33]. Considering that most maneuvering targets fly or perform maneuver inside the atmosphere, we transform the law in (22) into the form of

$$\begin{cases} \mathbf{a}_m = \dfrac{a_{m\theta}}{\mathbf{n}_m \cdot \mathbf{e}_\theta}\mathbf{n}_m, \\ a_{m\theta} = -\dot{r}\omega - \dot{r}\dfrac{d\nu_{\theta c}}{dr} + \alpha_1 x_2 + \alpha_2 x_2 \dfrac{d\beta(x_1)}{dx_1} + k_1 s + k_2|s|^\mu \operatorname{sgn}(s) + \dfrac{\widehat{\kappa}s}{2\varepsilon^2}, \end{cases} \tag{41}$$

where $\mathbf{a}_m$ is the missile guidance acceleration and $\mathbf{n}_m$ is a unit vector perpendicular to the missile velocity [5]. Thus, the transformed law is applicable to intercept the maneuvering target inside the atmosphere. In (41), to guarantee $\mathbf{n}_m \cdot \mathbf{e}_\theta \ne 0$, we assume

$$\mathbf{n}_m \cdot \mathbf{e}_\theta = \lambda, \tag{42}$$

where $0 < \lambda \le 1$. Moreover, $\mathbf{n}_m$ is subject to the constraints

$$\begin{cases} \mathbf{n}_m \cdot \mathbf{t}_m = 0, \\ |\mathbf{n}_m| = 1, \end{cases} \tag{43}$$

where $\mathbf{t}_m$ is the unit vector along the missile velocity. By combining (42) with (43), the existence condition for $\mathbf{n}_m$ is given as

$$1 - (\mathbf{t}_m \cdot \mathbf{e}_\theta)^2 \ge \lambda^2. \tag{44}$$

According to (44), λ is selected as follows:

$$\lambda = \sqrt{1 - (\mathbf{t}_m \cdot \mathbf{e}_\theta)^2} - \sigma, \tag{45}$$

where $\sigma > 0$ is sufficiently small. Then, two solutions can be achieved to $\mathbf{n}_m$ and denoted by $\mathbf{n}_{m1}$ and $\mathbf{n}_{m2}$. In view of the guidance command continuity, the solution should be adopted satisfying the following condition:

$$\mathbf{n}_m = \left\{\mathbf{n}_{mi} \mid \max\left[\cos < \mathbf{n}_{mi}, \mathbf{n}'_m > \right]; i = 1, 2\right\}, \tag{46}$$

where $\mathbf{n}'_m$ is $\mathbf{n}_m$ at previous moment. The above conversion is depicted in Figure 4 where $\nu = \arccos\lambda$.

4.4. Guidance Law Realization in Practical Interceptions. From (41) and the derivation, the involved guidance information includes the relative range r, the closing velocity $\dot{r}$, the LOSR ω, the unit vector $\mathbf{e}_\theta$, and the missile velocity vector $\mathbf{v}_m$. The missile seeker (usually Doppler radar or the combination with optical sensor) can directly obtain the

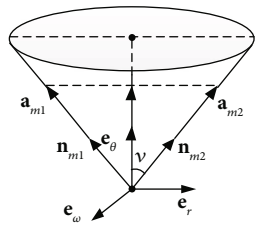

Figure 4: Guidance command conversion.

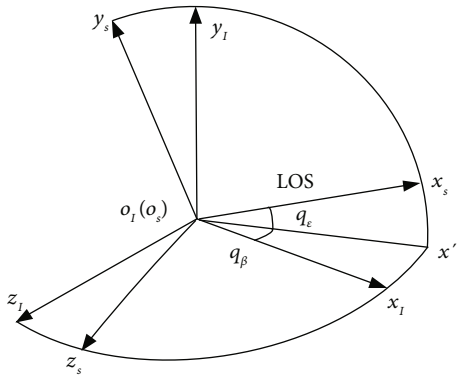

Figure 5: Relation between LOS angles and inertial reference system.

measurements as r, $\dot{r}$, the elevation angle q_ε, and the azimuth angle q_β of the LOS in the inertial reference system. The relation between the LOS angles and the inertial reference system is given in Figure 5. With filtering techniques, the LOS angle rates $\dot{q}_\varepsilon$ and $\dot{q}_\beta$ can be achieved.

From Figure 5, the angular velocity of the LOS coordinate system $o_s x_s y_s z_s$ is obtained as

$$\boldsymbol{\omega}_s = \begin{bmatrix} \cos q_\varepsilon & \sin q_\varepsilon & 0 \\ -\sin q_\varepsilon & \cos q_\varepsilon & 0 \\ 0 & 0 & 1 \end{bmatrix} \begin{bmatrix} 0 \\ \dot{q}_\beta \\ 0 \end{bmatrix} + \begin{bmatrix} 0 \\ 0 \\ \dot{q}_\varepsilon \end{bmatrix} = \begin{bmatrix} \dot{q}_\beta \sin q_\varepsilon \\ \dot{q}_\beta \cos q_\varepsilon \\ \dot{q}_\varepsilon \end{bmatrix}. \tag{47}$$

Thus, we have $\boldsymbol{\omega} = [0\ \dot{q}_\beta \cos q_\varepsilon\ \dot{q}_\varepsilon]^{\mathrm{T}} \neq$ which is equivalent to (2) in essence. Due to $\mathbf{e}_r = [1\ \ 0\ \ 0]^{\mathrm{T}}$, $\mathbf{e}_\theta$ has the form

$$\mathbf{e}_\theta = \mathbf{e}_\omega \times \mathbf{e}_r = \frac{1}{\omega} \begin{bmatrix} 0 \\ \dot{q}_\varepsilon \\ -\dot{q}_\beta \cos q_\varepsilon \end{bmatrix}, \tag{48}$$

where $\omega = \sqrt{(\dot{q}_\beta \cos q_\varepsilon)^2 + \dot{q}_\varepsilon^2}$. Notice that $\mathbf{v}_m$ can be measured or estimated by onboard inertial measurement unit or the combination with the satellite positioning system. Therefore, the designed guidance law is realizable in practical interceptions. The similar realization can be seen in [34].

Table 1: Required information of guidance laws.

Guidance law	Required information							
	r	$\dot{r}$	q_ε	q_β	$\dot{q}_\varepsilon$	$\dot{q}_\beta$	$\mathbf{t}_m$	$a_{t\theta}$
PTB-AGL	✓	✓	✓	✓	✓	✓	✓	✗
PTB-GL	✓	✓	✓	✓	✓	✓	✓	✗
OE-FTC-GL	✓	✓	✓	✓	✓	✓	✓	✗
PPN	✗	✗	✓	✓	✓	✓	✓	✗
TPN-C	✗	✓	✓	✓	✓	✓	✓	✗
ATPN-C	✗	✓	✓	✓	✓	✓	✓	✓

Note: ✓ denotes "the information is required"; ✗ denotes "the information is not required."

5. Simulations

In this section, a series of numerical simulations are conducted to examine the performance of the devised guidance law. As depicted in [8], the guidance command in (41) will be continuous and smooth via replacing sgn $(\cdot)$ by the sigmoid function

$$\mathrm{sgmf}(s) = 2\left(\frac{1}{1+\mathrm{e}^{-\chi s}} - \frac{1}{2}\right), \tag{49}$$

where χ is a positive constant. For simplicity, the modified law is abbreviated to PTB-AGL (profile-tracking-based adaptive guidance law). Meanwhile, the PTB-GL, where the adaptive term is removed from (41), the observed-embedded finite-time convergent guidance law (OE-FTC-GL) in [22], and the classical pure PN (PPN) in [2] are used to make comparisons. The latter two expressions are written as

$$\begin{cases} \mathbf{a}_{m\_\mathrm{PPN}} = N_1 \boldsymbol{\omega} \times \mathbf{v}_m, \\ \mathbf{a}_{m\_\mathrm{OE-FTC-GL}} = \dfrac{-N_2 \dot{r}\omega + \widehat{a}_{t\theta} + \alpha|\omega|^{\upsilon}\mathrm{sat}_{\delta_\omega}(\omega)}{\mathbf{n}_m \cdot \mathbf{e}_\theta} \mathbf{n}_m, \end{cases} \tag{50}$$

where $N_1 > 0$, $N_2 > 2$, $\alpha > 0$, $0 < \upsilon < 1$, $\widehat{a}_{t\theta}$ is the estimated value of $a_{t\theta}$ from an extended state observer, $\mathrm{sat}_{\delta_\omega}(\cdot)$ denotes the saturation function, and the approach to determining $\mathbf{n}_m$ is the same as in PTB-AGL. With the help of the command conversion, the true PN (TPN) in [35] and the augmented TPN (ATPN) in [5] are converted into the following forms:

$$\begin{cases} \mathbf{a}_{m\_\mathrm{TPN\text{-}C}} = \dfrac{-N_3 \dot{r}\omega}{\mathbf{n}_m \cdot \mathbf{e}_\theta} \mathbf{n}_m, \\ \mathbf{a}_{m\_\mathrm{ATPN\text{-}C}} = \dfrac{a_{t\theta} - N_3 \dot{r}\omega}{\mathbf{n}_m \cdot \mathbf{e}_\theta} \mathbf{n}_m, \end{cases} \tag{51}$$

where $N_3 > 2$. Then, TPN-C and ATPN-C are same as PPN in terms of the command direction, which can take part in the comparison with PTB-AGL. The required information of the above-mentioned laws is listed in Table 1. In ATPN-C, the target maneuver information is included which is difficult to be achieved in most cases. Hence, ATPN-C is almost unrealizable in practice and only for comparison here.

Table 2: Initial state of missile and target.

Initial state	Missile	Target
Position (km)	(2, 8, 0.5)	(12, 4, 1.5)
Velocity (m/s)	(1101.24, -459.84, 125.76)	(500, 0, 0)

In order to reflect the realistic intercept, maximum acceleration constraint and command lag from autopilot are taken into account. The missile acceleration is restricted as

$$\mathbf{a}_m = \begin{cases} \mathbf{a}_m, & \text{if } |\mathbf{a}_m| \le a_{\max}, \\ a_{\max} \dfrac{\mathbf{a}_m}{|\mathbf{a}_m|}, & \text{if } |\mathbf{a}_m| > a_{\max}, \end{cases} \tag{52}$$

where $a_{\max}$ is the maximum achievable value of the missile acceleration magnitude. The missile autopilot dynamics is considered as a first-order differential equation in the form of

$$\dot{a}_{ma} = -\frac{1}{\varpi} a_{ma} + \frac{1}{\varpi} a_{mc}, \tag{53}$$

where a_{ma} and a_{mc} are the delayed and commanded acceleration, respectively, and ϖ is the time constant. To evaluate control efforts of the guidance laws, an energy consumption function is defined as

$$J = \int_{t_0}^{t} |\mathbf{a}_m| \mathrm{d}\tau. \tag{54}$$

In addition, ΔJ is defined as the total energy consumption during the guidance process, that is, $\Delta J = J(t_f)$, where t_f is the final time of guidance. The simulations below are performed on a laptop with Intel Core i5-3470 3.20 GHz CPU. The result in this section is obtained by using MATLAB 2016a.

5.1. Case 1: Pursuing a Low-Velocity Maneuverable Target. The first set of simulations is carried out for the case where a missile with a velocity advantage is pursuing a maneuverable target. The initial state of the missile and the target in $o_I x_I y_I z_I$ is given in Table 2.

Three different types of target motion are considered as follows: (1) constant velocity (CV): $\mathbf{a}_t = (0, 0, 0)$; (2) constant maneuvering (CM): $\mathbf{a}_t = (0, 3g_0, 4g_0)$, $g_0 = 9.80665$ m/s^2; and (3) sinusoidal maneuvering (SM): $\mathbf{a}_t = (0, 3g_0, 5g_0 \cos 0.5t)$. The simulation step is 1 ms when $r \ge 2$ km and 0.1 ms when $r < 2$ km. The simulation terminates when $\dot{r} > 0$, and the miss distance is defined as the minimum value of r. The missile acceleration is limited by $a_{\max} = 10g_0$. The seeker blind-zone distance is selected as 100 m, and the guidance command keeps unchanged when r is less than the distance. The time constant of the autopilot dynamics is set as 0.1 s. At the initial time t_0, $\mathbf{n}_m$ = (0.3948, 0.9092, -0.1324), and $\widehat{\kappa} = 0$ are adopted. The key parameter settings involved in the guidance laws are listed in Table 3, and the other parameters for modification are chosen as $\delta = 0.05r_0$, $\sigma = 0.01$, and $\chi = 5$.

Table 3: Parameter settings for guidance laws.

Guidance law	Parameter
PTB-AGL	$a = 0.5$, $b = 0.05$, $\alpha_1 = \alpha_2 = 2$, $\gamma = 0.8$, $\xi = 0.01$, $k_1 = k_2 = 2$, $\mu = 0.1$, $k_3 = 0.1$, $k_4 = 0.001$, $\varepsilon = 0.8$
OE-FTC-GL	$N_1 = 3.0$, $\alpha = 10.0$, $\upsilon = 0.1$, $\delta_\omega = 5.0 \times 10^{-4}$
PPN/TPN-C	$N_2 = N_3 = 3.0$

Based on the above conditions, the simulation results are presented in Figures 6(a)–6(j) and Table 4. In Figure 6(d), the profile-tracking error of PTB-AGL rapidly converges to a small neighborhood of zero in comparison to that of PTB-GL, especially when against the CM and SM targets. This indicates that the addition of the adaptive term can better reject the target maneuver disturbance in PTB-AGL. It can be seen in Figure 6(e) that all the laws are able to reduce the LOSR to a low level in terms of intercepting the CV target. In addition, the least energy is consumed in PPN from Table 4. However, when dealing with the maneuvering targets, PPN and TPN-C, compared with the other four laws, cannot suppress the LOS rotation well because the target maneuver disturbance is not addressed. Thus, as shown in Table 4, they have larger miss distance and total energy consumption. Because of the direct target maneuver compensation, ATPN-C is significantly better than TPN-C. The histories of the guidance acceleration command are plotted in Figures 6(f)–6(h). When intercepting the SM target, the command of PTB-AGL is smooth while the unexpected chattering emerges in PTB-GL and ATPN-C, which demonstrates that the designed adaptive term works well. The CPU time costs of the laws are presented in Figure 6(j) where PTB-AGL has an advantage over OE-FTC-GL. This may be because an additional observer for estimation is required in OE-FTC-GL while the target maneuver is addressed by a simply adaptive term in PTB-AGL. PPN possesses the least time cost as predicted, but the unsatisfactory miss distance when against the SM target.

According to the above results, the guidance performance of PTB-AGL is superior to those of PTB-GL, PPN, TPN-C, and ATPN-C and, regardless of the CPU cost, comparable to that of OE-FTC-GL where the unknown target maneuver is accurately estimated and compensated due to the employment of the true guidance information. In addition, the convergence rate of the LOSR can be flexibly and quantitatively regulated by adjusting a. By contrast, OE-FTC-GL can only roughly control the convergence time of the LOSR because of the guidance scheme and the uncontrollable estimation error. The time histories of the LOSR under the different profile parameters are presented in Figure 7(a) where the convergence rate of the LOSR is flexibly controlled. Figure 7(b) shows the trends of the guidance performance versus the profile parameter at a proper interval. It can be observed that the miss distance always fluctuates within a low level and the total energy consumption varies with a. For intercepting a

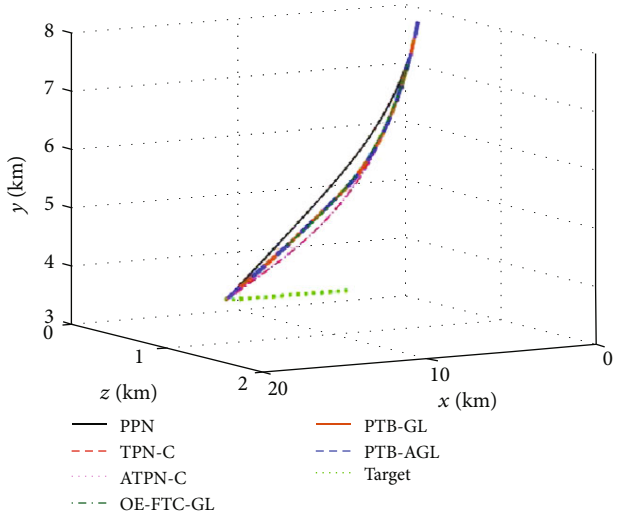

(a) Intercept trajectories (CV)

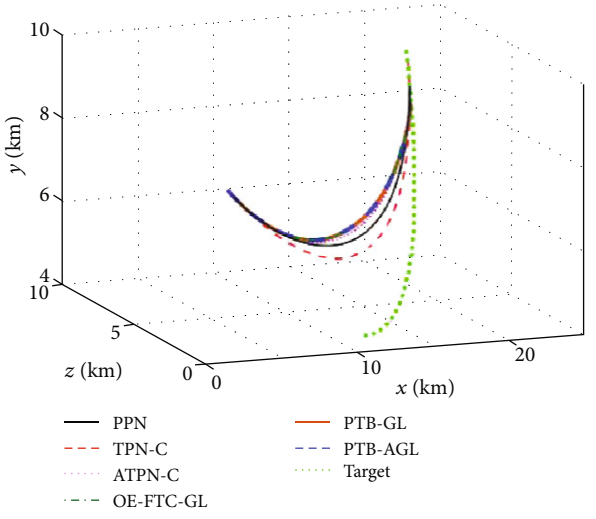

(b) Intercept trajectories (CM)

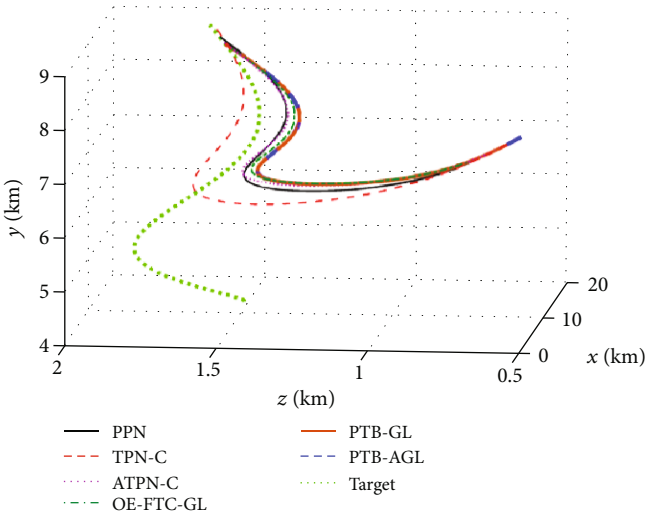

(c) Intercept trajectories (SM)

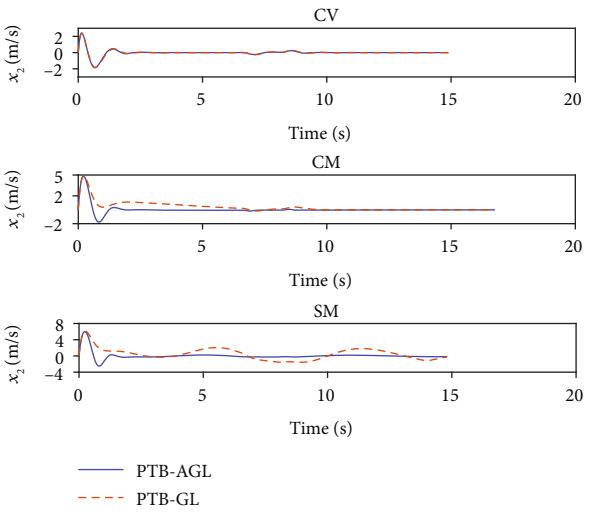

(d) Profile-tracking error versus time

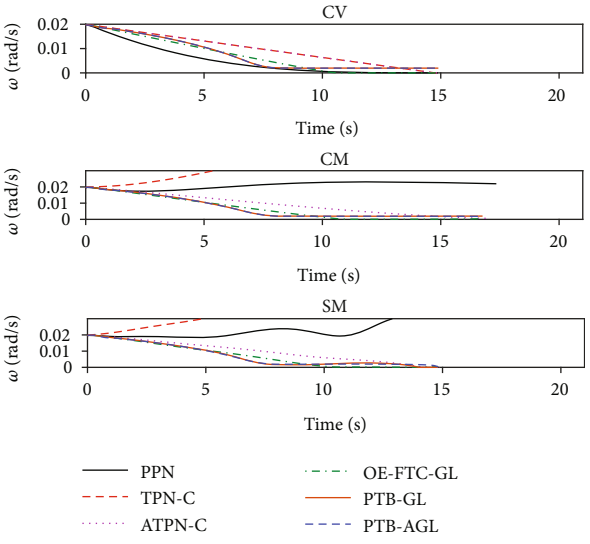

(e) LOSR versus time

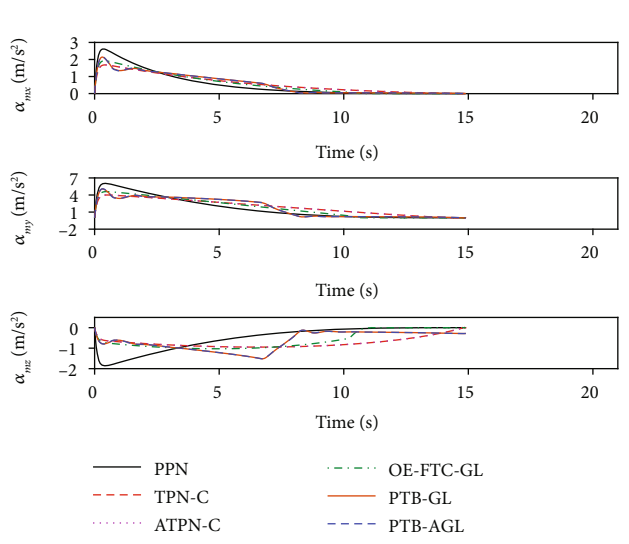

(f) Guidance acceleration versus time (CV)

Figure 6: Continued.

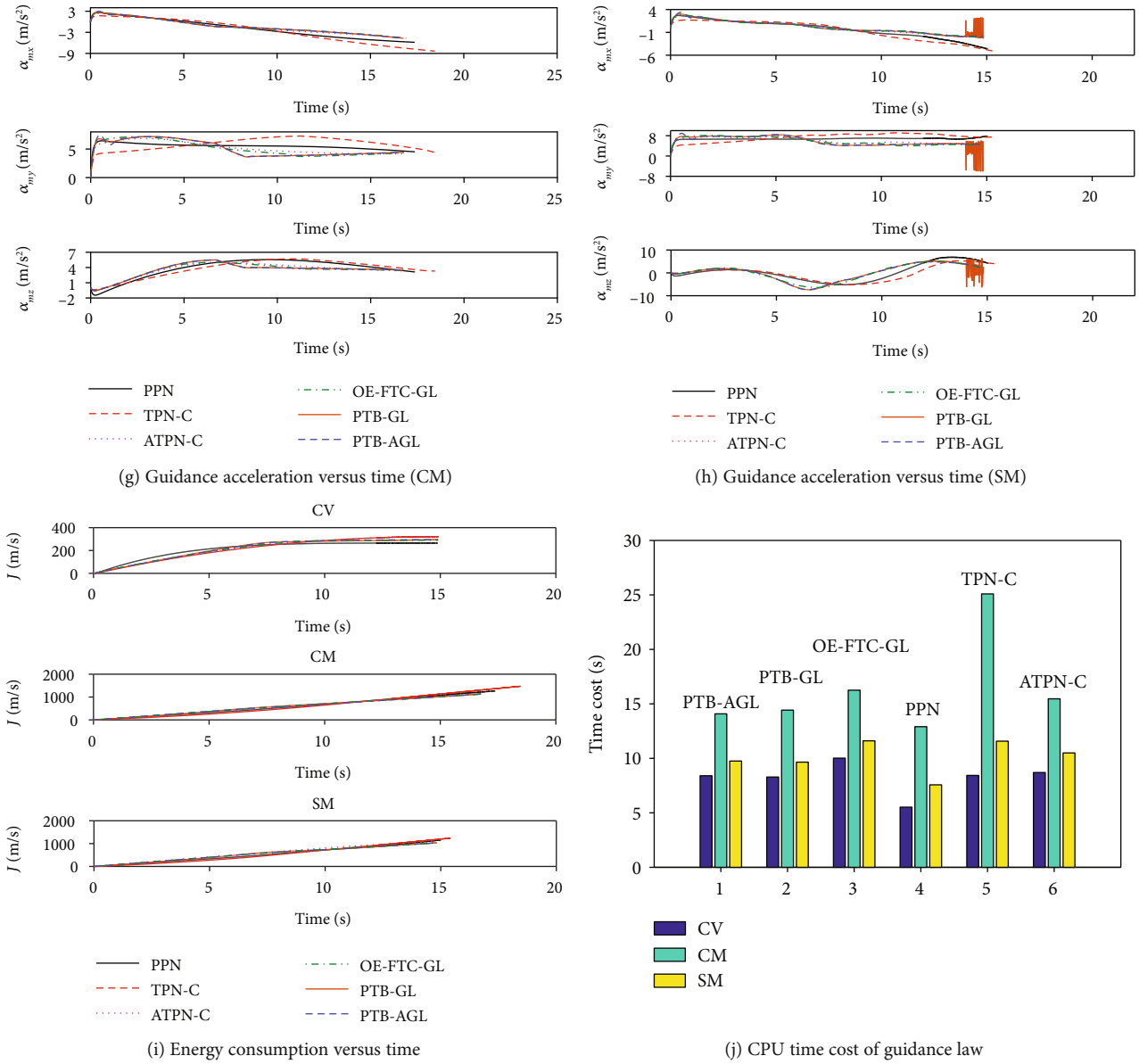

(g) Guidance acceleration versus time (CM)

(h) Guidance acceleration versus time (SM)

(i) Energy consumption versus time

(j) CPU time cost of guidance law

Figure 6: Simulation results under Case 1.

Table 4: Summary of guidance performance—Case 1.

Guidance law	Miss distance (m)			Total energy consumption (m/s)		
	CV	CM	SM	CV	CM	SM
PTB-AGL	0.0042	0.0116	0.0222	294.99	1148.87	1037.89
PTB-GL	0.0048	0.0158	0.1234	294.99	1149.48	1044.18
OE-FTC-GL	0.0325	0.0241	0.0175	289.03	1146.27	1036.69
PPN	0.0206	0.0276	4.4362	266.20	1323.66	1174.06
TPN-C	0.0141	59.9252	74.5088	321.11	1525.42	1252.22
ATPN-C	0.0141	0.0075	0.1555	321.11	1182.19	1061.31

maneuverable target, PTB-AGL can easily give a proper convergence rate via a when the energy consumption is taken into account.

5.2. Case 2: Head-On Intercepting a High-Velocity Maneuverable Target. In this subsection, an engagement scenario is constructed where a missile with a velocity

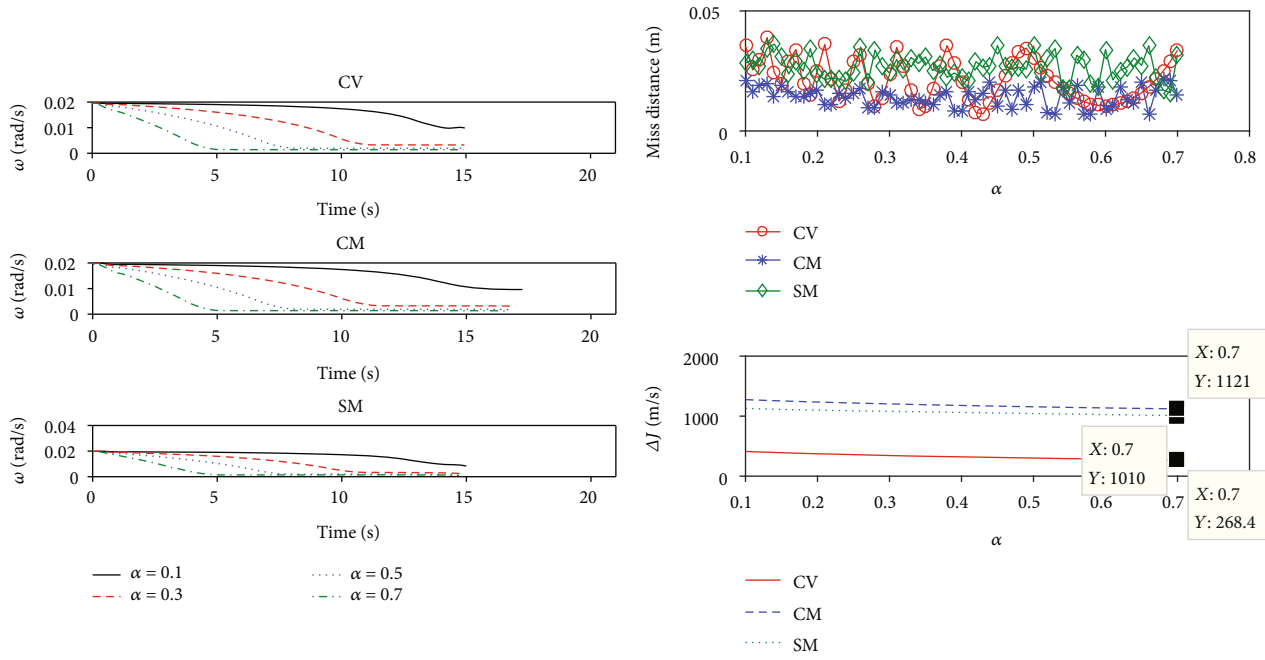

(a) LOSRs versus time with different a

(b) Guidance performance versus a

Figure 7: Intercept characteristics with profile parameter—Case 1.

Table 5: Initial state of the missile and the target.

Initial state	Missile	Target
Position (km)	(45, 10, 1)	(5, 15, 1.5)
Velocity(m/s)	(1691.10, 497.52, 364.14)	(2400, 0, 0)

disadvantage is head-on intercepting a high-velocity maneuverable target. The initial state of the missile and the target in $o_I x_I y_I z_I$ is given in Table 5.

Similarly, three different patterns of target motion are considered as follows: (1) CV: $\mathbf{a}_t = (0, 0, 0)$; (2) CM: $\mathbf{a}_t = (0, 2g_0, 3g_0)$; and (3) SM: $\mathbf{a}_t = (0, 2g_0, 4g_0 \cos 0.5t)$. The simulation step jumps to 0.1 ms when $r < 5$ km. The missile acceleration is limited by $a_{\max} = 12g_0$, and the seeker blind-zone distance is set as 300 m. At the initial time t_0, $\mathbf{n}_m = (-0.1369, 0.2383, -0.9615)$ is adopted. The parameters for the guidance laws are the same as in the previous subsection expect for $\delta = 0.1r_0$ and $b = 0.1$.

With the above conditions, the simulation results are shown in Figures 8(a)–8(j) and Table 6. From Figure 8(d), the adaptive term in PTB-AGL dramatically enhances the tracking precision of the profile, as shown in Figure 6(d). In Figure 8(e), PPN has no capacity to control the rotation of the LOS, which leads to the target missing as listed in Table 6. Likewise, the guidance acceleration of PTB-AGL is always smooth in Figures 8(f)–8(h). By contrast, ATPN-C, OE-FTC-GL, and PTB-GL yield different levels of chattering against the maneuvering targets. In terms of the energy consumption, PTB-AGL is less than TPN-C, especially when against the CM and SM targets, since the target maneuver is not considered in TPN-C. Therefore, the performance of PTB-AGL is preferable to the other four laws. Figure 8(j) gives the CPU time cost of the each law. It can be found from Figures 6(j) and 8(j) that the CPU cost is larger when intercepting the maneuvering targets, which mirrors the difficulty of dealing with maneuvering targets to some extent.

Figures 9(a)–9(b) give the time histories of the LOSR under the different profile parameters and the variations of the guidance performance versus the profile parameter, respectively. Generally, the parameter a should not be too large in view of finite tracking capability. As same as in Figure 7(a), the LOSR convergence rate of PTB-AGL can be regulated easily through adjusting a moderately in Figure 9(a). In Figure 9(b), the miss distance is kept at a low level, and the trend of the total energy consumption is different in terms of the different maneuvering types of targets. It is indicated that lowering the LOSR excessively requires more overload consumption when intercepting the CM target.

5.3. Monte Carlo Simulations with Measurement Noises. In the previous simulations, the guidance laws are implemented in a perfect scenario without measurement noise. However, in realistic scenarios, the required guidance information is inevitably contaminated with inherently noisy sensors. To examine the robustness of PTB-AGL, Monte Carlo simulations of Case 2 are conducted consisting of 500 sample runs. For the performance comparison, OE-FTC-GL is also examined. The measurement noises of the relative distance r and the closing velocity $\dot{r}$ are taken as normal distributions with zero mean and triple standard deviation of 100 m and 10 m/s, respectively, and those of the LOS angle and the LOS angle rate are zero

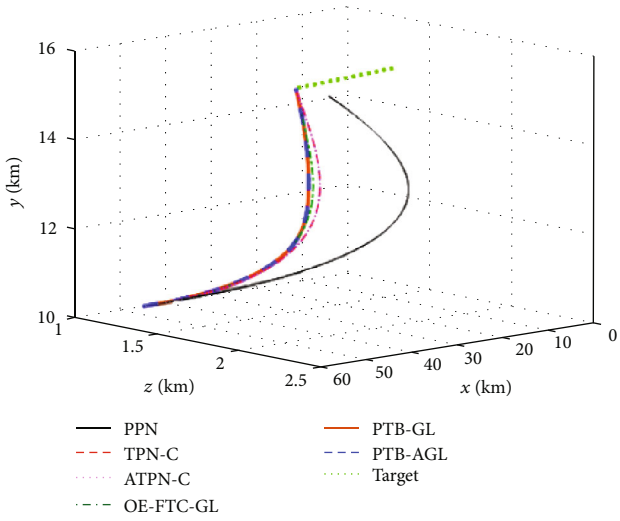

(a) Intercept trajectories (CV)

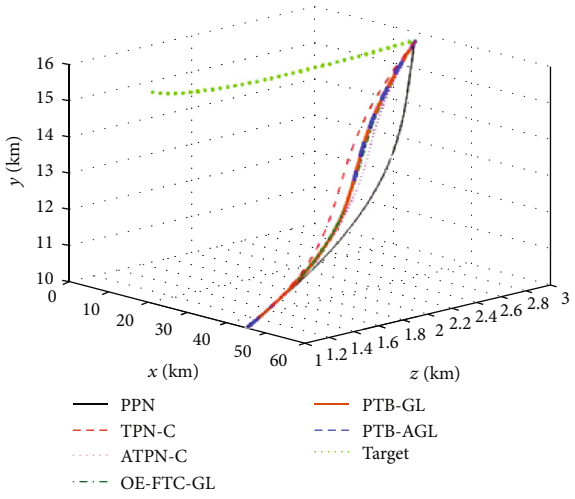

(b) Intercept trajectories (CM)

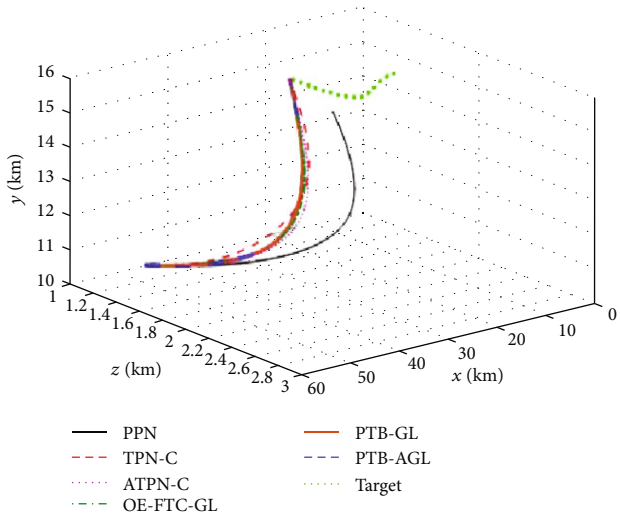

(c) Intercept trajectories (SM)

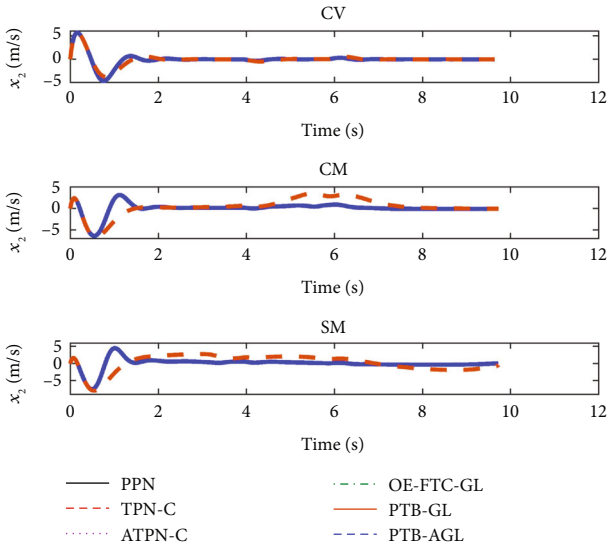

(d) Profile-tracking error versus time

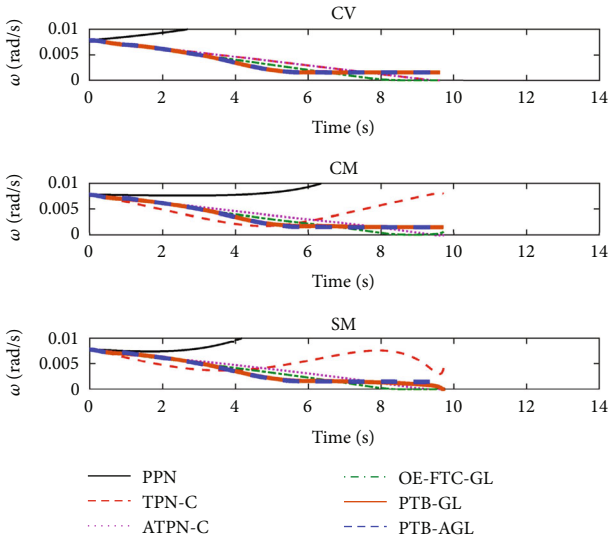

(e) LOSR versus time

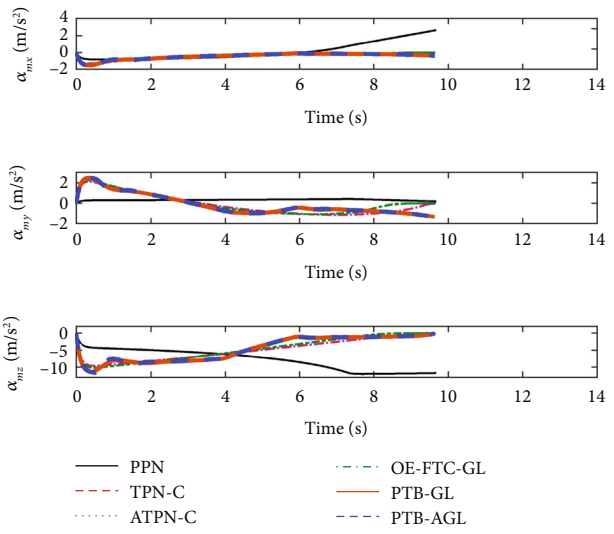

(f) Guidance acceleration versus time (CV)

Figure 8: Continued.

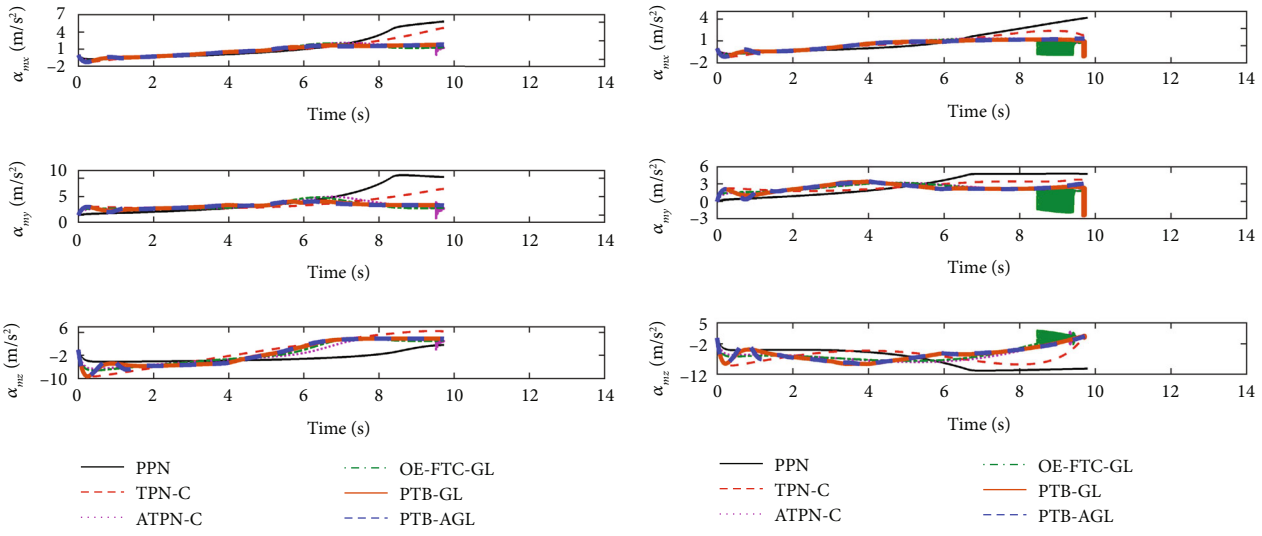

(g) Guidance acceleration versus time (CM)

(h) Guidance acceleration versus time (SM)

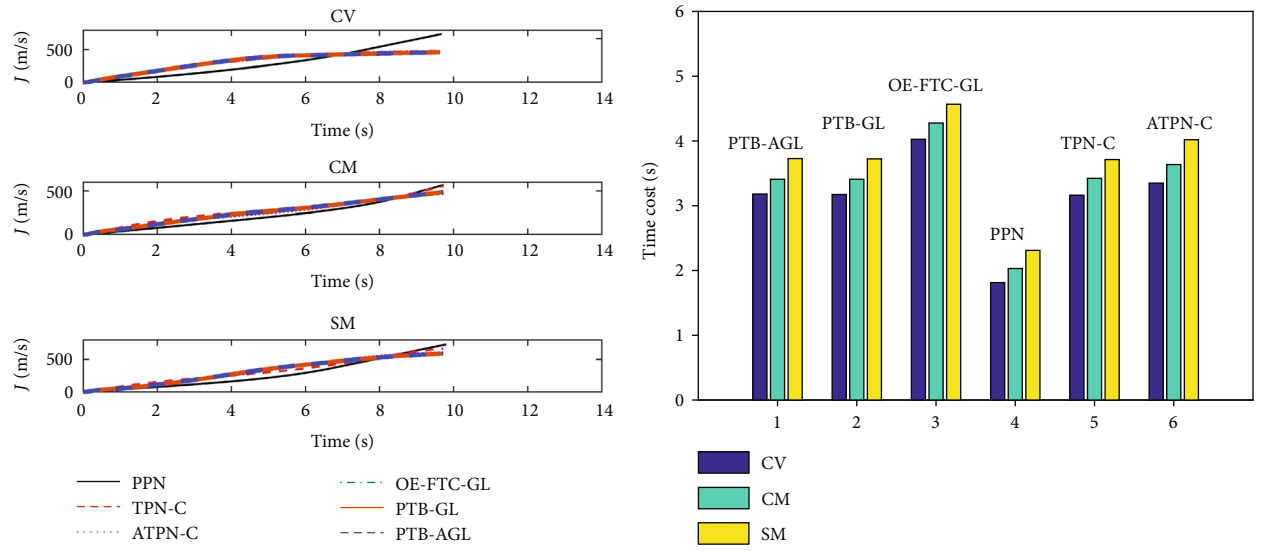

(i) Energy consumption versus time

(j) CPU time cost of guidance law

Figure 8: Simulation results under Case 2.

Table 6: Summary of guidance performance—Case 2.

Guidance law	Miss distance (m)			Total energy consumption (m/s)		
	CV	CM	SM	CV	CM	SM
PTB-AGL	0.1682	0.1455	0.0291	462.41	492.34	592.21
PTB-GL	0.1615	0.1641	0.1875	462.43	492.17	589.86
OE-FTC-GL	0.0730	0.0442	0.1322	455.15	472.23	591.76
PPN	193.6181	91.5074	495.5556	749.64	579.92	730.59
TPN-C	0.1831	0.0106	0.0800	478.04	564.50	668.25
ATPN-C	0.1831	0.1507	0.1338	478.04	476.30	609.25

mean and triple standard deviation of 0.1 deg and 0.01 deg/s, respectively. The measurement frequency of seeker is 50 Hz. According to Figure 9(b), the value of a is modified into 0.5, 0.4, and 0.6 when intercepting the CV, CM, and SM targets, respectively, and the other simulation settings are the same as in Case 2.

The Monte Carlo simulation results of the miss distance and the total energy consumption are presented in

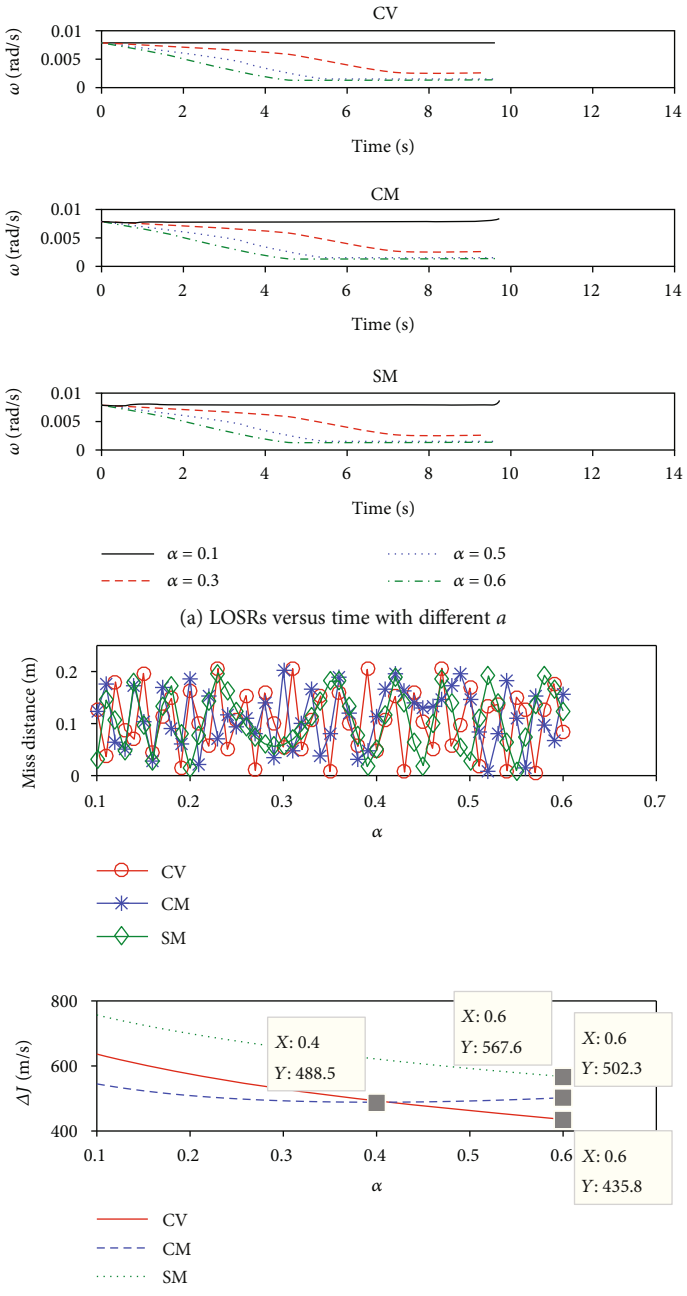

(a) LOSRs versus time with different a

(b) Guidance performance versus a

Figure 9: Intercept characteristics with profile parameter—Case 2.

Figure 10. The RMS values of the results are summarized in Table 7. It can be seen that the performance of PTB-AGL is satisfactory in the Monte Carlo sense, and largely better than that of OE-FTC-GL when intercepting the SM target.

6. Conclusions

In this paper, the terminal guidance problem for a hit-to-kill missile is addressed with demands for antichattering and quantitatively controlling the convergence rate of the LOSR. The proposed guidance law can precisely intercept maneuvering targets without chattering and the information of target maneuver. The performance is superior to the existing guidance laws, especially the traditional PPN. The conclusions are summarized as follows:

(1) The combination of the nonsingular fast terminal SMC and the adaptive algorithm can reject the disturbance of target maneuver well. It is realized that the tracking error of the profile rapidly converges to a small neighborhood of zero in finite time and the convergence rate of the LOSR can be regulated flexibly and quantitatively

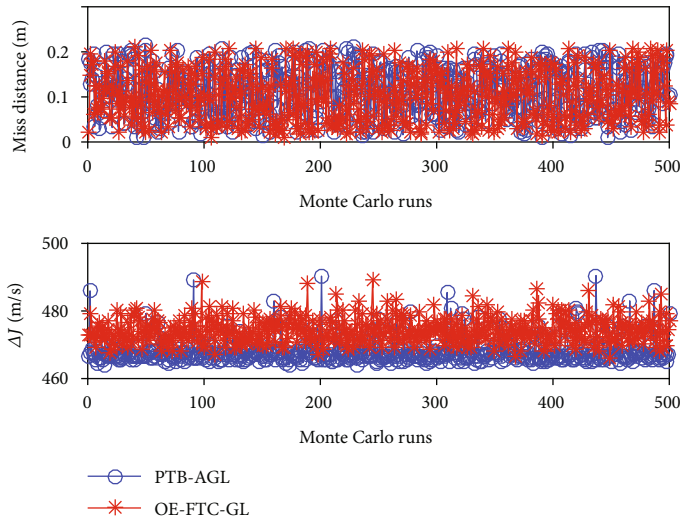

(a) Monte Carlo results (CV)

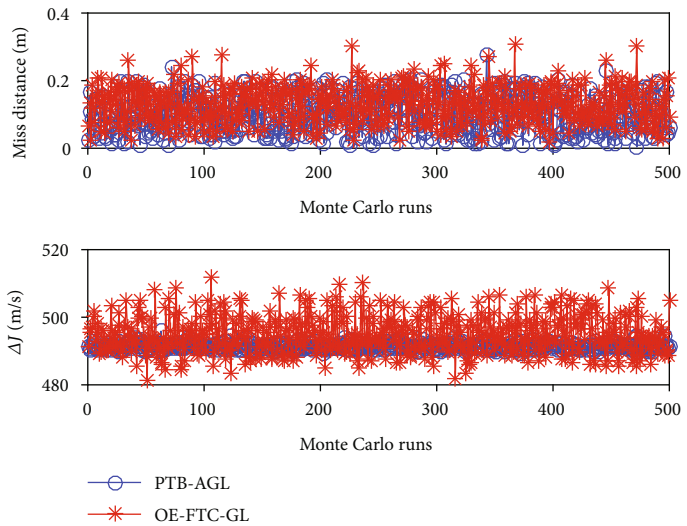

(b) Monte Carlo results (CM)

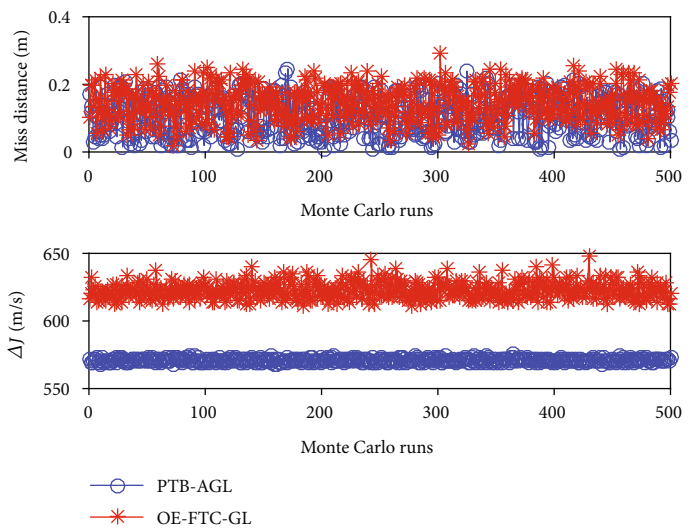

(c) Monte Carlo results (SM)

Figure 10: Monte Carlo results—Case 2.

Table 7: RMS values of Monte Carlo results—Case 2.

Guidance law	Miss distance (m)			Total energy consumption (m/s)		
	CV	CM	SM	CV	CM	SM
PTB-AGL	0.1256	0.1148	0.1205	468.29	491.33	570.94
OE-FTC-GL	0.1175	0.1417	0.1548	474.28	494.95	622.55

(2) The guidance-command-conversion scheme works well and can be served as a bridge from the law normal to the LOS to the one normal to missile velocity

(3) Reducing the LOSR as fast as possible may require more control efforts. When energy consumption is taken into account, PTB-AGL can give an appropriate convergence rate of the LOSR with respect to a maneuverable type of target

Data Availability

The data used in my manuscript is constructed by ourselves according to scenarios to be researched and completely shown in details in the manuscript. No additional data is involved.

Conflicts of Interest

The authors declare that there is no conflict of interests regarding the publication of this paper.

Acknowledgments

This paper was sponsored by the Aerospace Science and Technology Foundation of China Aerospace Science and Industry Corporation Limited 2017-HT-GF-07.

References

[1] N. A. Shneydor, *Missile Guidance and Pursuit: Kinematics, Dynamics and Control*, Horwood Publishing, Chichester, UK, 1998.

[2] C.-D. Yang and C.-C. Yang, "A unified approach to proportional navigation," *IEEE Transactions on Aerospace and Electronic Systems*, vol. 33, no. 2, pp. 557–567, 1997.

[3] J. Ye, H. Lei, and J. Li, "Novel fractional order calculus extended PN for maneuvering targets," *International Journal of Aerospace Engineering*, vol. 2017, Article ID 5931967, 9 pages, 2017.

[4] P. Zarchan, *Tactical and Strategic Missile Guidance*, American Institute of Aeronautics and Astronautics, Inc., Reston, VA, USA, 2012.

[5] K. B. Li, L. Chen, and X. Z. Bai, "Differential geometric modeling of guidance problem for interceptors," *Science China Technological Sciences*, vol. 54, no. 9, pp. 2283–2295, 2011.

[6] D. Zhou, C. Mu, and W. Xu, "Adaptive sliding-mode guidance of a homing missile," *Journal of Guidance, Control, and Dynamics*, vol. 22, no. 4, pp. 589–594, 1999.

[7] J. Moon, K. Kim, and Y. Kim, "Design of missile guidance law via variable structure control," *Journal of Guidance, Control, and Dynamics*, vol. 24, no. 4, pp. 659–664, 2001.

[8] S. R. Kumar, S. Rao, and D. Ghose, "Sliding-mode guidance and control for all-aspect interceptors with terminal angle constraints," *Journal of Guidance, Control, and Dynamics*, vol. 35, no. 4, pp. 1230–1246, 2012.

[9] S. Sun, D. Zhou, J. Zhou, and K. L. Teo, "A generalized design method for three-dimensional guidance laws," *Proceedings of the Institution of Mechanical Engineers, Part G: Journal of Aerospace Engineering*, vol. 231, no. 1, pp. 47–60, 2016.

[10] Y. Wang, S. Tang, W. Shang, and J. Guo, "Adaptive fuzzy sliding mode guidance law considering available acceleration and autopilot dynamics," *International Journal of Aerospace Engineering*, vol. 2018, Article ID 6081801, 10 pages, 2018.

[11] S. He, D. Lin, and J. Wang, "Integral global sliding mode guidance for impact angle control," *IEEE Transactions on Aerospace and Electronic Systems*, vol. 55, no. 4, pp. 1843–1849, 2019.

[12] C. S. Shieh, "Design of three-dimensional missile guidance law via tunable nonlinear H_∞ control with saturation constraint," *IET Control Theory & Applications*, vol. 1, no. 3, pp. 756–763, 2007.

[13] D. Zhou and B. Xu, "Adaptive dynamic surface guidance law with input saturation constraint and autopilot dynamics," *Journal of Guidance, Control, and Dynamics*, vol. 39, no. 5, pp. 1155–1162, 2016.

[14] D. Zhou, S. Sun, and K. L. Teo, "Guidance laws with finite time convergence," *Journal of Guidance, Control, and Dynamics*, vol. 32, no. 6, pp. 1838–1846, 2009.

[15] S. Sun, D. Zhou, and W. T. Hou, "A guidance law with finite time convergence accounting for autopilot lag," *Aerospace Science and Technology*, vol. 25, no. 1, pp. 132–137, 2013.

[16] H. S. Shin, A. Tsourdos, and K. B. Li, "A new three-dimensional sliding mode guidance law variation with finite time convergence," *IEEE Transactions on Aerospace and Electronic Systems*, vol. 53, no. 5, pp. 2221–2232, 2017.

[17] Z. Zhang, S. Li, and S. Luo, "Terminal guidance laws of missile based on ISMC and NDOB with impact angle constraint," *Aerospace Science and Technology*, vol. 31, no. 1, pp. 30–41, 2013.

[18] B. Zhao and J. Zhou, "Smooth adaptive finite time guidance law with impact angle constraints," *International Journal of Aerospace Engineering*, vol. 2016, Article ID 5730168, 19 pages, 2016.

[19] V. T. Haimo, "Finite time controllers," *SIAM Journal on Control and Optimization*, vol. 24, no. 4, pp. 760–770, 1986.

[20] Y. Hong, J. Huang, and Y. Xu, "On an output feedback finite-time stabilization problem," *IEEE Transactions on Automatic Control*, vol. 46, no. 2, pp. 305–309, 2001.

[21] S. Yu, X. Yu, B. Shirinzadeh, and Z. Man, "Continuous finite-time control for robotic manipulators with terminal sliding mode," *Automatica*, vol. 41, no. 11, pp. 1957–1964, 2005.

[22] H. B. Zhou, S. M. Song, and J. H. Song, "Design of sliding mode guidance law with dynamic delay and impact angle constraint," *International Journal of Control, Automation and Systems*, vol. 15, no. 1, pp. 239–247, 2017.

[23] Y. W. Ma and W. H. Zhang, "Differential geometric guidance command with finite time convergence using extended state observer," *Journal of Central South University*, vol. 23, no. 4, pp. 859–868, 2016.

[24] Z. Zhang, C. Man, S. Li, and S. Jin, "Finite-time guidance laws for three-dimensional missile-target interception," *Proceedings of the Institution of Mechanical Engineers, Part G: Journal of Aerospace Engineering*, vol. 230, no. 2, pp. 392–403, 2015.

[25] Y. J. Si and S. M. Song, "Adaptive reaching law based three-dimensional finite-time guidance law against maneuvering targets with input saturation," *Aerospace Science and Technology*, vol. 70, pp. 198–210, 2017.

[26] X. Wang and J. Wang, "Partial integrated guidance and control with impact angle constraints," *Journal of Guidance, Control, and Dynamics*, vol. 38, no. 5, pp. 925–936, 2015.

[27] J. Wang and S. He, "Optimal integral sliding mode guidance law based on generalized model predictive control," *Proceedings of the Institution of Mechanical Engineers, Part I: Journal of Systems and Control Engineering*, vol. 230, no. 7, pp. 610–621, 2016.

[28] V. Behnamgol, A. R. Vali, and A. Mohammadi, "A new adaptive finite time nonlinear guidance law to intercept maneuvering targets," *Aerospace Science and Technology*, vol. 68, pp. 416–421, 2017.

[29] J. Zhou and J. Yang, "Smooth sliding mode control for missile interception with finite-time convergence," *Journal of Guidance, Control, and Dynamics*, vol. 38, no. 7, pp. 1311–1318, 2015.

[30] Y. L. Zhang, Y. Xie, S. C. Peng, G. J. Tang, and W. M. Bao, "Entry trajectory generation with complex constraints based on three- dimensional acceleration profile," *Aerospace Science and Technology*, vol. 91, pp. 231–240, 2019.

[31] J. Song, S. Song, and H. Zhou, "Adaptive nonsingular fast terminal sliding mode guidance law with impact angle constraints," *International Journal of Control, Automation and Systems*, vol. 14, no. 1, pp. 99–114, 2016.

[32] U. S. Shukla and P. R. Mahapatra, "The proportional navigation dilemma-pure or true?," *IEEE Transactions on Aerospace and Electronic Systems*, vol. 26, no. 2, pp. 382–392, 1990.

[33] K. B. Li, L. Chen, and G. J. Tang, "Improved differential geometric guidance commands for endoatmospheric interception of high-speed targets," *Science China Technological Sciences*, vol. 56, no. 2, pp. 518–528, 2013.

[34] K.-B. Li, W. S. Su, and L. Chen, "Performance analysis of differential geometric guidance law against high-speed target with arbitrarily maneuvering acceleration," *Proceedings of the Institution of Mechanical Engineers, Part G: Journal of Aerospace Engineering*, vol. 233, no. 10, pp. 3547–3563, 2018.

[35] K. B. Li, Y. G. Liang, W. S. Su, and L. Chen, "Performance of 3D TPN against true-arbitrarily maneuvering target for exoatmospheric interception," *Science China Technological Sciences*, vol. 61, no. 8, pp. 1161–1174, 2018.